ACCEPTED FOR PUBLICATION IN APJ
Preprint typeset using LaTeX style emulateapj v. 08/22/09

ASTEROSEISMOLOGY OF RED GIANTS FROM THE FIRST FOUR MONTHS OF *KEPLER* DATA: GLOBAL OSCILLATION PARAMETERS FOR 800 STARS

D. Huber[1], T. R. Bedding[1], D. Stello[1], B. Mosser[2], S. Mathur[3], T. Kallinger[4,5], S. Hekker[6], Y. P. Elsworth[6], D. L. Buzasi[7], J. De Ridder[8], R. L. Gilliland[9], H. Kjeldsen[10], W. J. Chaplin[6], R. A. García[11], S. J. Hale[6], H. L. Preston[7,12], T. R. White[1], W. J. Borucki[13], J. Christensen-Dalsgaard[10], B. D. Clarke[14], J. M. Jenkins[14], and D. Koch[13]

accepted for publication in ApJ

ABSTRACT

We have studied solar-like oscillations in ~ 800 red-giant stars using *Kepler* long-cadence photometry. The sample includes stars ranging in evolution from the lower part of the red-giant branch to the Helium main sequence. We investigate the relation between the large frequency separation ($\Delta\nu$) and the frequency of maximum power ($\nu_{\rm max}$) and show that it is different for red giants than for main-sequence stars, which is consistent with evolutionary models and scaling relations. The distributions of $\nu_{\rm max}$ and $\Delta\nu$ are in qualitative agreement with a simple stellar population model of the Kepler field, including the first evidence for a secondary clump population characterized by $M \gtrsim 2\,M_{\odot}$ and $\nu_{\rm max} \simeq 40-110\,\mu$Hz. We measured the small frequency separations $\delta\nu_{02}$ and $\delta\nu_{01}$ in over 400 stars and $\delta\nu_{03}$ in over 40. We present C-D diagrams for $l = 1$, 2 and 3 and show that the frequency separation ratios $\delta\nu_{02}/\Delta\nu$ and $\delta\nu_{01}/\Delta\nu$ have opposite trends as a function of $\Delta\nu$. The data show a narrowing of the $l = 1$ ridge towards lower $\nu_{\rm max}$, in agreement with models predicting more efficient mode trapping in stars with higher luminosity. We investigate the offset ϵ in the asymptotic relation and find a clear correlation with $\Delta\nu$, demonstrating that it is related to fundamental stellar parameters. Finally, we present the first amplitude-$\nu_{\rm max}$ relation for *Kepler* red giants. We observe a lack of low-amplitude stars for $\nu_{\rm max} \gtrsim 110\,\mu$Hz and find that, for a given $\nu_{\rm max}$ between $40 - 110\,\mu$Hz, stars with lower $\Delta\nu$ (and consequently higher mass) tend to show lower amplitudes than stars with higher $\Delta\nu$.

Subject headings: stars: oscillations — stars: late-type

1. INTRODUCTION

Stars with convective envelopes show solar-like oscillations that are sensitive to the physical processes governing their interiors (see, e.g., Brown & Gilliland 1994; Christensen-Dalsgaard 2004). Following the success of helioseismology, the detection of such oscillations in a variety of stars holds great promise for improving our understanding of stellar structure and evolution.

The traditional goal of asteroseismology is the accurate measurement of individual mode frequencies, which can be used to test stellar physics by comparing them to frequencies predicted by models. In a more general approach, global oscillation parameters can be used. These include the average frequency separations, which are directly related to properties of the sound speed in the stellar interior and therefore to fundamental stellar parameters. Other parameters are the amplitude and central frequency of the oscillation envelope, which are important for understanding the physics of driving and damping of these modes. The measurement of these parameters presents a valuable addition to classical methods such as spectroscopy, and a powerful tool to systematically study stellar evolution when oscillations are detected in a large ensemble of stars.

Compared to main-sequence stars, red giants pulsate with larger amplitudes and longer periods, therefore requiring less sensitivity but longer and preferably continuous time series for unambiguous detections. The first attempts to detect oscillations in G and K giants were focused on nearby targets such as Arcturus (Smith 1983; Cochran 1988; Belmonte et al. 1990). This was followed by campaigns targeting single stars and clusters using precise ground-based Doppler spectroscopy (Frandsen et al. 2002; De Ridder et al. 2006) and photometry (Stello et al. 2007), as well as using space-based photometers such as the *HST* (Edmonds & Gilliland 1996; Gilliland 2008; Stello & Gilliland 2009), *WIRE* (Buzasi

[1] Sydney Institute for Astronomy (SIfA), School of Physics, University of Sydney, NSW 2006, Australia; dhuber@physics.usyd.edu.au
[2] LESIA, CNRS, Université Pierre et Marie Curie, Université Denis, Diderot, Observatoire de Paris, 92195 Meudon cedex, France
[3] High Altitude Observatory, NCAR, P.O. BOX 3000, Boulder, CO 80307, USA
[4] Department of Physics and Astronomy, University of British Columbia, Vancouver, Canada
[5] Institute of Astronomy, University of Vienna, 1180 Vienna, Austria
[6] School of Physics and Astronomy, University of Birmingham, Edgbaston, Birmingham B15 2TT, UK
[7] Eureka Scientific, 2452 Delmer Street Suite 100, Oakland, CA 94602-3017, USA
[8] Instituut voor Sterrenkunde, K.U.Leuven, Belgium
[9] Space Telescope Science Institute, 3700 San Martin Drive, Baltimore, Maryland 21218, USA
[10] Danish AsteroSeismology Centre (DASC), Department of Physics and Astronomy, Aarhus University, DK-8000 Aarhus C, Denmark
[11] Laboratoire AIM, CEA/DSM-CNRS, Université Paris 7 Diderot, IRFU/SAp, Centre de Saclay, 91191, Gif-sur-Yvette, France
[12] Department of Mathematical Sciences, University of South Africa, Box 392 UNISA 0003, South Africa
[13] NASA Ames Research Center, MS 244-30, Moffett Field, CA 94035, USA
[14] SETI Institute, NASA Ames Research Center, MS 244-30, Moffett Field, CA 94035, USA

et al. 2000; Retter et al. 2003; Stello et al. 2008), *MOST* (Barban et al. 2007; Kallinger et al. 2008a,b) and *SMEI* (Tarrant et al. 2007).

A breakthrough was achieved by *CoRoT* with unambiguous detections of radial and non-radial modes in $\sim$800 red giants (De Ridder et al. 2009; Hekker et al. 2009; Carrier et al. 2010). With a maximum time series length of 150 d but limitations due to the low-Earth orbit of the satellite, the *CoRoT* detections were focused on low-mass He-core burning stars (the red clump). Using these data, Miglio et al. (2009) performed the first population study using global oscillation parameters and concluded that the distributions were qualitatively in agreement with the current picture of the star formation rate in our galaxy. Mosser et al. (2010) subsequently used a larger number of detections in the *CoRoT* sample to investigate correlations of various oscillation parameters.

A new era of "ensemble asteroseismology" was recently entered with the launch of the *Kepler* space telescope (Gilliland et al. 2010). First results for red giants were based on 34 d of data (Bedding et al. 2010b; see also Stello et al. 2010; Hekker et al. 2010c) which demonstrated the enormous potential of *Kepler* data. While Bedding et al. (2010b) focused on a sample of low-luminosity giants, the goal of this paper is to systematically investigate global oscillation parameters in the complete *Kepler* red-giant sample using data spanning up to 138 d. We refer to our companion papers for the comparison of global oscillation parameters derived using different methods (Hekker et al. 2010b) and the asteroseismic determination of stellar masses and radii (Kallinger et al. 2010b).

2. OBSERVATIONS AND DATA ANALYSIS

The *Kepler* space telescope was launched in March 2009 with the principal science goal of detecting Earth-like planets around solar-like stars through the observation of photometric transits. *Kepler* employs two observation modes, sampling data either in 1 min (short-cadence) or 29.4 min (long-cadence) intervals. For our study of pulsations in red giants we used *Kepler* long-cadence data (Jenkins et al. 2010), which have a Nyquist frequency of 283 μHz.

Kepler is located in an Earth-trailing orbit with spacecraft rolls performed at quarterly intervals to redirect solar panels towards the Sun. Data are consequently subdivided into quarters, starting with the initial commissioning run (10 d, Q0), followed by a short first quarter (34 d, Q1) and a full second quarter (90 d, Q2). The basis of our study consists of 1531 light curves for which data from all these quarters are available (total time span of 137.9 d). We did not include stars thought to be members of the open clusters in the *Kepler* field (NGC6791, NGC6811, NGC6819 and NGC6866).

Before we extracted asteroseismic information from the time series, two main instrumental artifacts had to be addressed. Firstly, in some cases data from different quarters show intensity discontinuities that are mainly caused by pixel shifts after reorientation of the spacecraft (Jenkins et al. 2010). Additionally, two safe-mode events in Q2 caused intensity drifts due to thermal effects, affecting in total $\sim$7.5 days of the data. We discarded data affected by the safe-mode events and corrected for intensity jumps by robust fitting and correcting second-order polynomials to Q0, Q1 and five separate segments of Q2 which were unaffected by intensity jumps (see also Kallinger et al. 2010b). Finally, we performed a simple 4-σ outlier clipping to remove remaining outlying data points (in most cases $<0.1\%$ of the total number of data points).

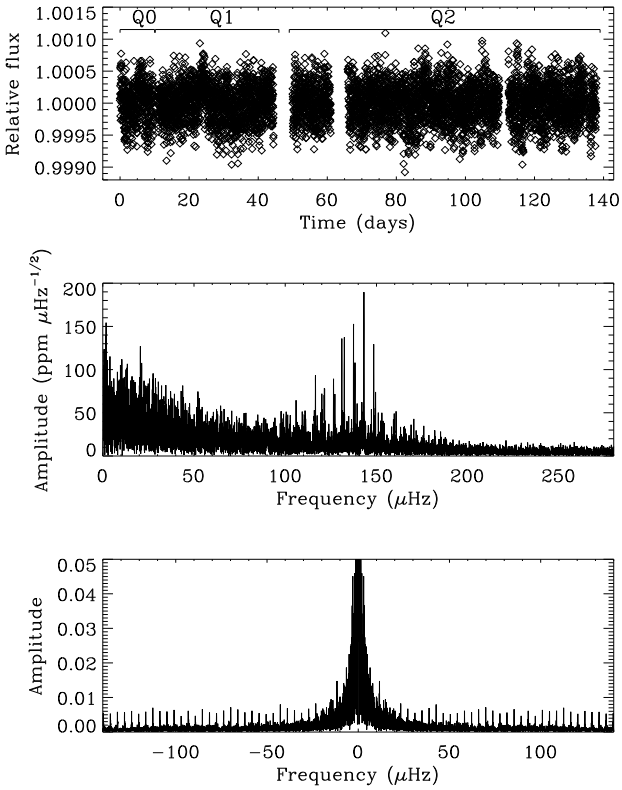

FIG. 1.— *Top panel: Kepler* light curve of the oscillating red giant KIC5515314. The different quarters of data used in this work are indicated. *Middle panel:* Amplitude spectrum of the light curve shown in the top panel. Note that the ordinate shows the square root of power density, where the latter is power multiplied by the effective length of the dataset (calculated as the inverse of the area under the spectral window). *Bottom panel:* Spectral window, shown at the same abscissa scale as the middle panel. Note that the height of the peak at zero frequency is 1.

The top panel of Figure 1 shows a typical light curve after the above corrections have been performed. The different quarters contributing to the final light curve are indicated. The main gaps in the datasets span 1.5 d between Q0 and Q1, 4.5 d between Q1 and Q2, and 5 d as well as 2.5 d during the aforementioned safe-mode events in Q2. The middle panel displays the amplitude spectrum of the light curve, showing the clear signature of solar-like oscillations with regularly spaced peaks centered around 130 μHz. The spectral window shown in the bottom panel of Figure 1 demonstrates the nearly continuous sampling of *Kepler* data. The weak peaks at multiples of 3.96 μHz are caused by the angular momentum dumping cycle of the spacecraft causing one rejected datapoint every 2.9 d. At a level of less than 1% in amplitude, these aliasing artifacts are negligible for the analysis considered in this paper.

To extract oscillation parameters from the corrected time series, several methods have been employed (Hekker et al. 2010d; Huber et al. 2009; Kallinger et al. 2010b;

Mathur et al. 2010; Mosser & Appourchaux 2009). For a detailed comparison of the results of these different methods we refer to Hekker et al. (2010b). Unless otherwise mentioned, all results shown here are based on the method by Huber et al. (2009). All values from that method were cross-checked with the others and we only retained stars for which at least one other method yielded consistent results. Uncertainties reported in this paper are based on calibrations of extensive ($\sim$50000) simulations of artificial time series with identical sampling to the *Kepler* data, including mixed modes, background noise and varying mode lifetimes between 15–75 d.

Before reporting our results, we provide a brief summary of the global oscillation parameters used in this work, their physical interpretation and the principal methods with which they were determined.

3. GLOBAL OSCILLATION PARAMETERS

3.1. *Frequency of maximum power ($\nu_{\rm max}$)*

As first argued by Brown et al. (1991), $\nu_{\rm max}$ for sun-like stars is expected to scale with the acoustic cut-off frequency and can therefore be related to fundamental stellar parameters, as follows (Kjeldsen & Bedding 1995):

$$\nu_{\rm max} = \frac{M/M_\odot (T_{\rm eff}/T_{\rm eff,\odot})^{3.5}}{L/L_\odot} \nu_{\rm max,\odot} \, . \qquad (1)$$

As shown by Stello et al. (2009) for stellar models and as observed in stars with well-determined fundamental parameters (see, e.g., Stello et al. 2008), this scaling relation also holds for red giants. In these stars, $\nu_{\rm max}$ is a good indicator of the evolutionary stage, and ranges from $\sim$10 μHz for high-luminosity giants to $\sim$250 μHz for H-shell-burning stars in the lower part of the red-giant branch. It is measured by determining the maximum of the power excess after heavily smoothing over several orders or by fitting a Gaussian function to the excess power.

To illustrate our sample, Figure 2 shows all stars in a plot of $\nu_{\rm max}$ versus $T_{\rm eff}$. Effective temperatures have been taken from the Kepler Input Catalog (KIC) (Latham et al. 2005) and we have overlaid solar-scaled ASTEC evolutionary tracks (Christensen-Dalsgaard 2008). In addition to the red giants, we also show a sample of main-sequence and sub-giant stars for which oscillations had been detected prior to the *Kepler* mission (see Stello et al. 2009, and references therein). Figure 2 can be viewed as an asteroseismic H-R diagram in which, in the absence of parallaxes, we have used $1/\nu_{\rm max}$ instead of luminosity. As can be seen from the evolutionary tracks in Figure 2, our sample spans a total range of masses of approximately 1–3 $M_\odot$, with temperatures ranging from 4200 to 5200 K. For a detailed study of the fundamental parameters of the stars in the sample we refer to our companion paper (Kallinger et al. 2010b).

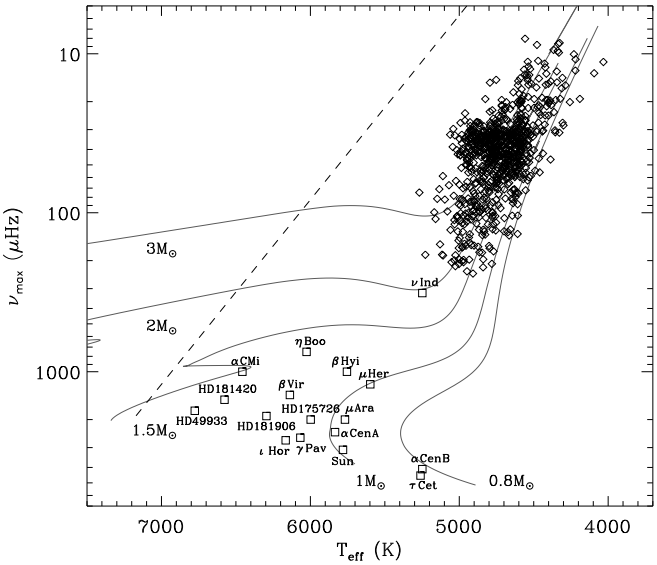

FIG. 2.— $\nu_{\rm max}$ versus effective temperature for all red giants in our sample (diamonds), as well as main-sequence and sub-giant stars studied by Stello et al. (2009) (squares). Error bars have been omitted for clarity. The grey lines show solar-metallicity ASTEC evolutionary tracks (Christensen-Dalsgaard 2008) for a range of masses (note that the 0.8 $M_\odot$ track has been evolved beyond the age of the universe). The dashed line marks the approximate position of the red edge of the instability strip.

3.2. *Frequency separations*

According to the asymptotic relation for modes of low angular degree l and high radial order n (Tassoul 1980; Gough 1986), frequencies of solar-like oscillations can be described by a series of characteristic separations. Observationally, these separations can be expressed as follows (Bedding & Kjeldsen 2010):

$$\nu_{n,l} = \Delta\nu (n + \frac{1}{2} l + \epsilon) - \delta\nu_{0l} \, . \qquad (2)$$

Here, $\Delta\nu$ denotes the mean large frequency separation of modes with the same degree and consecutive order. $\Delta\nu$ is directly related to the sound travel time across the stellar diameter and probes the mean stellar density (Ulrich 1986). This means that $\Delta\nu$ is expected to scale as follows:

$$\Delta\nu = \frac{(M/M_\odot)^{0.5} (T_{\rm eff}/T_{\rm eff,\odot})^3}{(L/L_\odot)^{0.75}} \Delta\nu_\odot \, . \qquad (3)$$

In Equation (2), $\delta\nu_{0l}$ denotes the small frequency separations of non-radial modes relative to radial modes, as follows:

$$\delta\nu_{02} = \nu_{n,0} - \nu_{n-1,2} \, , \qquad (4)$$

$$\delta\nu_{01} = \frac{1}{2}(\nu_{n,0} + \nu_{n+1,0}) - \nu_{n,1} \, , \qquad (5)$$

$$\delta\nu_{03} = \frac{1}{2}(\nu_{n,0} + \nu_{n+1,0}) - \nu_{n,3} \, . \qquad (6)$$

Following Bedding et al. (2010b), we have used $\delta\nu_{03}$ instead of the more commonly used $\delta\nu_{13}$ due to the broadening of the $l = 1$ ridge in red giants caused by mixed modes (Dupret et al. 2009; Deheuvels et al. 2010). For main-sequence stars, small frequency separations are sensitive to variations of the sound speed gradient near the stellar core, which changes as the star evolves due to the increase in its mean molecular weight.

The phase constant ϵ in Equation (2) has contributions from the inner and outer turning point of the modes. This is usually expressed as $\epsilon = \frac{1}{4} + \alpha$, where α is the

contribution from the outer turning point, which is determined by the properties of the near-surface region of the star (Christensen-Dalsgaard & Perez Hernandez 1992).

3.3. *Maximum mode amplitude*

The maximum mode amplitude is related to the turbulent convection mechanisms that excite and damp the oscillations. Kjeldsen & Bedding (1995) found that model predictions of solar-like oscillations by Christensen-Dalsgaard & Frandsen (1983) implied a scaling for velocity amplitudes of

$$v_{\rm osc} \propto \left(\frac{L}{M}\right)^{s} , \quad (7)$$

with $s = 1.0$ (see also Houdek et al. 1999). More recent calculations for main-sequence stars by Samadi et al. (2007) have favored an exponent of $s = 0.7$.

Kjeldsen & Bedding (1995) also argued that the oscillation amplitude A_λ observed in photometry at wavelength λ is related to the velocity amplitude:

$$A_\lambda \propto \frac{v_{\rm osc}}{\lambda} T_{\rm eff}^{-r} , \quad (8)$$

where $r = 1.5$ if the oscillations are adiabatic. However, Kjeldsen & Bedding (1995) found a better fit to observed amplitudes in classical pulsators with an exponent of $r = 2.0$.

Observationally, Stello et al. (2010) found agreement with $s = 0.7$ (assuming $r = 2.0$) for cluster red giants observed with *Kepler*, while Mosser et al. (2010) found a best fitting value of $s = 0.89 \pm 0.02$ (assuming $r = 1.5$) for *CoRoT* red giants. As for $\nu_{\rm max}$, mode amplitudes are usually determined by heavily smoothing the power spectrum to eliminate variations caused by the stochastic nature of the signal (Kjeldsen et al. 2008) or by fitting a Gaussian function to the power excess envelope. In both cases, it is important to determine an accurate fit to the stellar background contribution. To account for the effects of averaging from the 29.4 min integrations, we divided the observed amplitude with a sinc function: $A_{\rm real} = A_{\rm obs}/{\rm sinc}(\frac{\pi}{2}\frac{\nu_{\rm max}}{\nu_{\rm Nyq}})$.

4. RESULTS

4.1. *The $\Delta\nu$ - $\nu_{\rm max}$ relation*

The growing number of detections of solar-like oscillations across the HR diagram has revealed a tight power-law relation between $\Delta\nu$ and $\nu_{\rm max}$:

$$\Delta\nu = \alpha(\nu_{\rm max}/\mu{\rm Hz})^{\beta} . \quad (9)$$

Using a fit to red giants and main-sequence stars, Stello et al. (2009) derived $\alpha = 0.263 \pm 0.009\,\mu$Hz and $\beta = 0.772 \pm 0.005$, noting that models predicted slightly different relations for red giants than for main-sequence stars (see their Figure 3). The relation was also seen for the *CoRoT* red giants ($\nu_{\rm max} < 100\,\mu$Hz) by Hekker et al. (2009) and subsequently by Mosser et al. (2010), with the latter finding $\alpha = 0.28 \pm 0.02\,\mu$Hz and $\beta = 0.75 \pm 0.01$.

The *Kepler* data allow us to investigate this relation for the first time over a large part of the red giant branch. Figure 3 shows the relation for our sample. To derive the coefficients in Equation (9), we performed least-squares

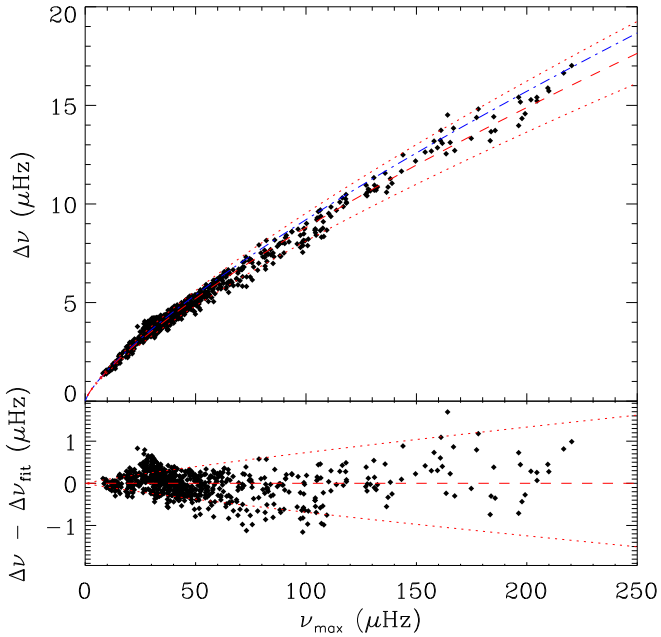

FIG. 3.— *Upper panel:* $\Delta\nu$ versus $\nu_{\rm max}$ for the *Kepler* red giants. The fitted relation is indicated by the red dashed line, with red dotted lines marking 3-σ uncertainties. The blue dashed-dotted line shows the relation by Stello et al. (2009). Note that the relation by Mosser et al. (2010) and the average relation for *Kepler* stars derived using seven different analysis methods are indistinguishable from the red dashed line. *Lower panel:* Residuals after subtracting the fit indicated by the red dashed line.

fits to the results of seven different methods. Note that we have omitted all stars with $\nu_{\rm max} > 230\,\mu$Hz from the analysis of the $\Delta\nu$-$\nu_{\rm max}$ relation due to the difficulty of determining accurate $\nu_{\rm max}$ values close to the Nyquist frequency. As can be seen in Table 1, there is good agreement between the results of different methods, as well as with the result by Mosser et al. (2010) that was based on *CoRoT* stars with $\nu_{\rm max} < 100\,\mu$Hz.

As already shown by Stello et al. (2009), a value of $\beta \sim 0.75$ is expected from the scaling relations for $\nu_{\rm max}$ and $\Delta\nu$. Raising Equation (1) to the power of 0.75 and dividing by Equation (3) yields

$$\frac{(\nu_{\rm max}/\mu{\rm Hz})^{0.75}}{\Delta\nu/\mu{\rm Hz}} \propto \left(\frac{M}{M_\odot}\right)^{0.25} \left(\frac{T_{\rm eff}}{T_{\rm eff,\odot}}\right)^{-0.375} . \quad (10)$$

This removes the dependence on luminosity and leaves only weak dependences on mass and effective temperature, with the latter only varying by a small amount on the red-giant branch.

As noted by Mosser et al. (2010), the difference between the relation for red giants and the one including main-sequence stars by Stello et al. (2009) is small but significant. To illustrate this difference we plot the relations together with observations and evolutionary tracks in Figure 4. Note that $\nu_{\rm max}$ and $\Delta\nu$ for the models have been calculated using equations (1) and (3). Compared to Figure 3, we replaced the ordinate in the upper panel by the ratio $\nu_{\rm max}/\Delta\nu$, which scales with the radial order of maximum power. The lower panel shows this ratio with $\nu_{\rm max}$ raised to the power of 0.75, which better illustrates the mass dispersion since in this plot, constant masses correspond to almost horizontal lines (see Equa-

TABLE 1
COEFFICIENTS OF THE $\Delta\nu$-$\nu_{\rm max}$ RELATION.

Source	α (μHz)	β	$\nu_{\rm max}$ (μHz)	# of stars
A2Z[1]	0.266±0.004	0.759±0.003	8–221	810
CAN[1]	0.286±0.004	0.745±0.003	12–228	893
COR[1]	0.279±0.004	0.749±0.003	2–208	1151
DLB[1]	0.293±0.009	0.747±0.008	1–192	256
OCTI[1]	0.273±0.004	0.752±0.003	14–208	829
OCTII[1]	0.254±0.004	0.764±0.003	16–203	829
SYD[1]	0.268±0.004	0.758±0.003	8-220	799
CoRoT[2]	0.28±0.02	0.75±0.01	2–100	1827
MS+RG[3]	0.263±0.009	0.772±0.005	15–4500	55

[1] *Kepler* red giants: A2Z - Mathur et al. (2010), CAN - Kallinger et al. (2010b), COR - Mosser & Appourchaux (2009), DLB - Buzasi et al. (unpublished), OCTI & OCTII - Hekker et al. (2010d), SYD - Huber et al. (2009).
[2] *CoRoT* red giants, see Mosser et al. (2010).
[3] Main-sequence (MS) and red giant (RG) stars, see Stello et al. (2009) and references therein.

tion (10)). The *Kepler* stars are shown in bins of 20 μHz (red diamonds). Note that the red giants used by Stello et al. (2009) have been omitted for clarity, but do not differ significantly from the *Kepler* sample. The uncertainties for the main-sequence sample have been collected from the literature where available or were set to typical values of 3% for $\nu_{\rm max}$ and 1% for $\Delta\nu$.

The scatter about the $\Delta\nu$-$\nu_{\rm max}$ relation is considerably larger than the measurement uncertainties (which are ∼1% for $\Delta\nu$ in our sample) and for red giants is mainly caused by the spread of stellar masses (Kallinger et al. 2010c). While Figure 4 shows that this spread is significant on the red-giant branch, it can be seen that the evolutionary tracks (solid lines) almost overlap for main-sequence stars. This effect causes a different fit to the relation between $\Delta\nu$ and $\nu_{\rm max}$ for a sample consisting only of red giants compared to when main-sequence stars are included, which is clearly reflected by the observations and the determined fits shown in Figure 4.

The dotted and dashed triple-dotted lines in Figure 4 illustrate the effect of changing the metallicity for the 1 $M_\odot$ track. The effect is relatively small on the giant branch (Kallinger et al. 2010c), but more significant for less evolved stars. In fact, both main-sequence stars significantly above the Stello et al. (2009) relation, η Boo and μ Her, are observed to be metal-rich (Carrier et al. 2005; Yang & Meng 2010), while the sub-giant ν Indi which falls below the relation is metal-poor (Bedding et al. 2006). Hence, these observations are qualitatively in agreement with expectations from evolutionary models combined with scaling relations.

A detailed investigation of these effects using pulsation models (which would be necessary to quantify mass and metallicity changes in Figure 4 in absolute terms) is beyond the scope of this paper. However, our results show that the observed difference in the $\Delta\nu$-$\nu_{\rm max}$ relation for red giants compared to when main-sequence stars are included is consistent with scaling relations. A more detailed investigation of the relation for main-sequence stars using *Kepler* short-cadence data will be presented in a forthcoming paper.

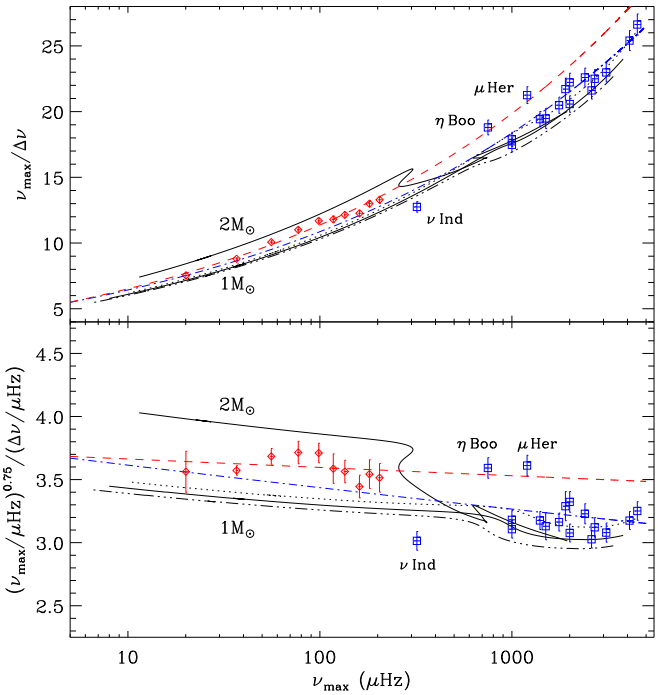

FIG. 4.— *Upper panel:* Solar-metallicity (Y=0.283, Z=0.017) evolutionary tracks (solid lines) together with the relation by Stello et al. (2009) (blue dashed-dotted line) and the relation fitted to the *Kepler* data (red dashed line). Blue squares show the main-sequence and sub-giant stars used by Stello et al. (2009), and red diamonds the *Kepler* observations as shown in Figure 3 in bins of 20 μHz. The black dashed triple-dotted and dotted lines show the solar-mass tracks for chemical compositions of (Y,Z) = (0.291,0.009) and (Y,Z) = (0.265,0.035), respectively. *Lower panel:* Same as the upper panel, but with the luminosity dependence of the ordinate removed by raising $\nu_{\rm max}$ to the power of 0.75 (see Equation (10)).

4.2. *Population effects in the $\nu_{\rm max}$ and $\Delta\nu$ distributions*

The large number and diversity of red giants for which solar-like oscillations have been detected enables us to identify stellar populations using global oscillation parameters. Due to the straightforward relationship between oscillation parameters and fundamental parameters (see equations (1) and (3)), comparisons with models could allow us to draw some conclusions about the star-formation history in the *Kepler* field. Such studies have already been performed for red giants observed by *CoRoT* (Miglio et al. 2009; Yang et al. 2010).

Before such a comparison is made, it is important to consider potential biases in the sample of *Kepler* red giants. Firstly, limitations on the bandwidth of spacecraft communications restrict the number of stars for which data can be obtained. Hence, absolute star counts for a given field and magnitude range will be incomplete. Secondly, about two thirds of the *Kepler* red-giant sample have been chosen as astrometric reference stars (Batalha et al. 2010; Monet et al. 2010). These have been selected to be distant, bright but unsaturated giants ($T_{\rm eff,KIC} < 5400$ K, $\log g_{\rm KIC} < 3.8$, $R/R_{\odot,\rm KIC} > 2$) in the *Kepler* magnitude range 11.0–12.5. Through the remainder of this paper we will refer to these stars as the astrometric sample, and to the remaining stars as the asteroseismic sample. Thirdly, as was the case for the *CoRoT* sample, the *Kepler* sample excludes stars pul-

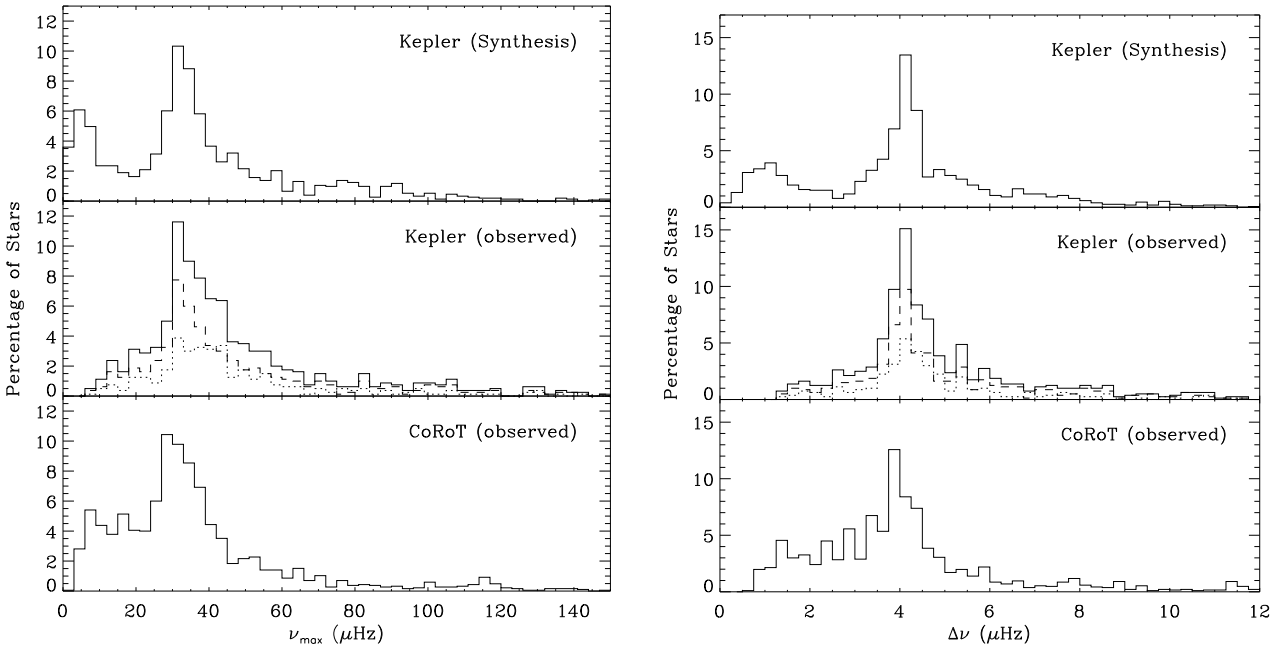

FIG. 5.— Histograms of $\nu_{\rm max}$ (left panels) and $\Delta\nu$ (right panels) in percent comparing a synthetic stellar population for the *Kepler* FOV (top panels), the observed distributions in the *Kepler* sample (middle panels) and the observed distributions in the *CoRoT* sample (bottom panels). The dashed and dotted lines in the middle panel separately show the distributions of the astrometric and asteroseismic sample, respectively. Note that the comparison for the *Kepler* sample should be restricted to stars with $\nu_{\rm max} \gtrsim 10\,\mu$Hz ($\Delta\nu \gtrsim 1.5\,\mu$Hz).

sating at frequencies that are too low to be resolved with the given time base available at this stage of the mission ($\nu_{\rm max} \lesssim 10\,\mu$Hz).

To obtain a first qualitative analysis of the observed distributions of the *Kepler* sample, we calculated a synthetic stellar population the same way as Miglio et al. (2009), using the stellar synthesis code TRILEGAL (Girardi et al. 2005). The input parameters were identical to the simulations performed by Miglio et al. (2009) for the *CoRoT* sample, with the exception of restricting the simulation to a 10 deg^2 field centered on the Kepler FOV (α=290.7°, δ=44.5°) in the magnitude range 8 – 13 mag in the *Kepler* bandpass. A constant star-formation rate was assumed.

Figure 5 compares the distributions of the synthetic *Kepler* population with the observed one, together with the *CoRoT* sample (Mosser et al. 2010). Note that the latter includes stars from both fields of view of *CoRoT*, one directed to the galactic center, the other to the galactic anti-center. As for the *CoRoT* sample, we observe a maximum at $\nu_{\rm max} \sim 30\,\mu$Hz, corresponding to the red clump. These are low-mass ($< 2 M_{\odot}$) stars, for which He-core burning occurs at similar luminosities (and hence similar $\nu_{\rm max}$), forming a dominant population on the giant branch. Miglio et al. (2009) noted that for the *CoRoT* stars, the maximum appears at a lower value of $\nu_{\rm max}$ (higher luminosity) than for the model. This is not the case for the *Kepler* field.

The dashed and dotted lines in the middle panel show the distributions of the astrometric and asteroseismic sample separately, to illustrate potential biases introduced in the overall distribution by combining these distinctly selected sets of stars. We see that the red clump maximum is predominantly formed by the astrometric sample, while the asteroseismic sample contributes more to slightly higher $\nu_{\rm max}$ values. This suggests that the astrometric sample is largely unbiased, while the broadening of the red clump peak compared to the model is potentially caused by selection bias in the asteroseismic sample.

Apart from the red clump, a second and much broader component in the synthetic population can be identified in the interval $\nu_{\rm max} \simeq 40-110\,\mu$Hz and $\Delta\nu \simeq 5-10\,\mu$Hz. This consists of more massive stars that, compared to the red clump, occupy lower luminosities (and hence higher $\nu_{\rm max}$) over a wider range when they settle as He-core burning stars. This component is referred to as the secondary clump by Girardi (1999). A comparison with the histogram of the *Kepler* sample shows that the observations qualitatively reproduce the distributions for both higher $\nu_{\rm max}$ and $\Delta\nu$ values.

To investigate this further, Figure 6 shows the ratio $\nu_{\rm max}/\Delta\nu$ as a function of $\nu_{\rm max}$ for the synthetic population and for the *Kepler* observations. The solid lines are evolutionary tracks of different masses. Figure 7 shows the same plot but with the luminosity dependence on the ordinate removed by raising $\nu_{\rm max}$ to the power of 0.75. In both figures, the separation of the red clump and the secondary clump is obvious in the population synthesis (upper panels). For the observations (lower panels) we can identify a group of stars with $M > 2\,M_{\odot}$ extending up to $\nu_{\rm max} \sim 110\,\mu$Hz, as expected for the secondary clump population.

The qualitative agreement between the distributions is encouraging and the excess of stars with $\nu_{\rm max} = 40 - 110\,\mu$Hz and $M > 2\,M_{\odot}$ suggests that the *Kepler* sample includes stars belonging to the secondary clump population. As pointed out by Girardi (1999), the detection of these stars should allow us to probe important physics, such as convective-core overshooting, and help to put tight constraints on the recent star-formation history in the galaxy. The detailed modelling required for

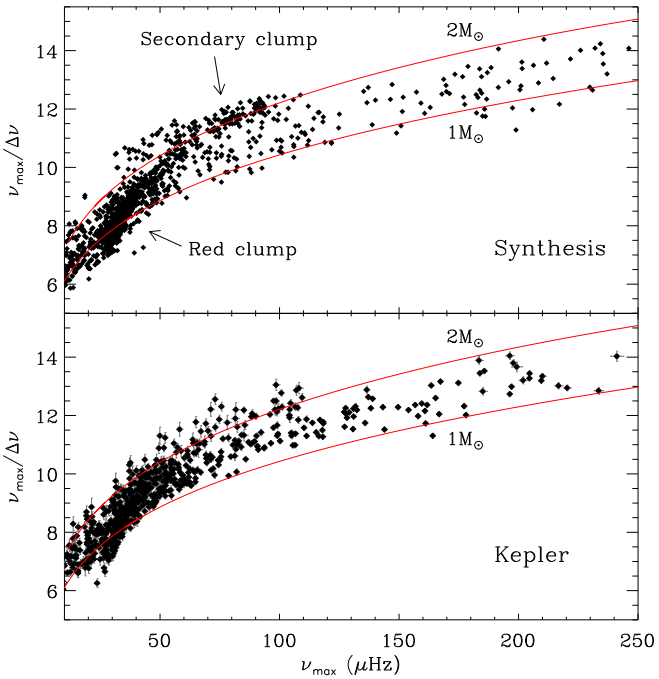

FIG. 6.— Ratio of $\nu_{\rm max}/\Delta\nu$ as a function of $\nu_{\rm max}$ for the synthetic population (upper panel, 1530 stars) and the *Kepler* red-giant sample (lower panel, 801 stars). Red lines show solar-metallicity (Y=0.283, Z=0.017) ASTEC evolutionary tracks with masses as indicated in the plots. The red clump and secondary clump populations are indicated for the synthetic population.

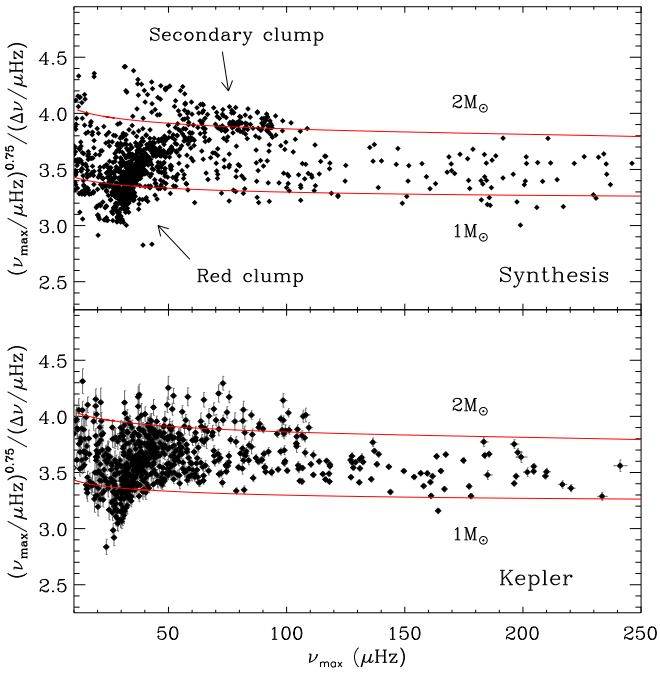

FIG. 7.— Same as Figure 6, but with the luminosity dependence of the ordinate removed by raising $\nu_{\rm max}$ to the power of 0.75 (see Equation (10)).

these inferences is beyond the scope of this paper.

4.3. *Small frequency separations*

As discussed in Section 3.2, the small frequency separations of main-sequence stars depend on the sound-speed gradient in the stellar core and are sensitive to the evolutionary state of a star. The excellent quality of the *Kepler* data allows us to measure the small separations in an unprecedented number of stars covering a wide range of evolutionary states on the giant branch.

To measure the small separations, we first examined the échelle diagram of each star using the power spectrum in the frequency range $\nu_{\rm max} \pm 5\Delta\nu$ and then manually fine-tuned the large separation to make the $l = 0$ ridge vertical. The adjustment to $\Delta\nu$ was typically a few tenths of a microhertz. Stars for which no unambiguous identification of $l = 0$ and 2 could be found were discarded from this analysis. The adjusted échelle diagram was then collapsed, and a Gaussian function was fitted to each mode ridge that was identified. The center of the fitted Gaussian was taken as the position of that ridge. Using this technique we were able to measure the $l = 0$ and 2 ridges for 470 stars. Of these, we measured the $l = 1$ ridge for 400 stars and the $l = 3$ ridge for 45 stars. The uncertainties were determined from extensive simulations of artificial *Kepler* data that were analyzed using the same method. Before discussing the separations of the ridges, we first consider their absolute positions.

4.3.1. *Variation of ϵ*

The measured mode ridge centroids allow us to investigate the parameter ϵ in Equation (2). Guided by the Sun, for which $\epsilon \simeq 1.5$ (see, e.g., Equation (11) in Kjeldsen & Bedding 1995), we have plotted the centroid positions in Figure 8, which shows that ϵ is a function of $\Delta\nu$.

Figure 8 also shows a considerable spread in ϵ for a given $\Delta\nu$, in particular for stars with $\Delta\nu < 5\,\mu$Hz. While the spread is of the same order as the estimated uncertainties, we have tested whether some of it might be related to physical properties of the stars. We have investigated this by correlating ϵ with $\nu_{\rm max}/\Delta\nu$ which, as shown in Figure 6, is sensitive to stellar mass. No clear correlation could be found.

The relation between ϵ and $\Delta\nu$ (and hence also $\nu_{\rm max}$) implies that ϵ is a function of fundamental parameters. If this relation can be quantified for less-evolved stars, clear mode ridge identifications as presented in this paper could potentially be used to predict ϵ for other stars. As suggested by Bedding & Kjeldsen (2010), such comparisons can be of considerable help in cases where the mode ridge identification is difficult due to short mode lifetimes or rotational splitting (see, e.g., Appourchaux et al. 2008; Benomar et al. 2009; García et al. 2009; Kallinger et al. 2010a; Bedding et al. 2010a).

Meanwhile, we can already use the ensemble results in Figure 8 to suggest ridge identifications for the four *CoRoT* red giants discussed by Hekker et al. (2010a). These stars have $\Delta\nu$ in the range 3.1 to 5.3 μHz and so we expect ϵ to be 1.0 or slightly less. Looking at the échelle diagrams of these stars (see Figures 8, 10, 12 and 14 in Hekker et al. 2010a), we indeed see in all cases that one of the two ridges falls there. In each of these diagrams, this indicates it is the left-hand ridge that corresponds to $l = 1$ and the other to $l = 0$.

4.3.2. *C-D diagrams*

Using the measured mode ridge centroids, we were able to derive the small separations $\delta\nu_{02}$, $\delta\nu_{01}$ and $\delta\nu_{03}$ for 470, 400 and 45 stars, respectively. The results are shown

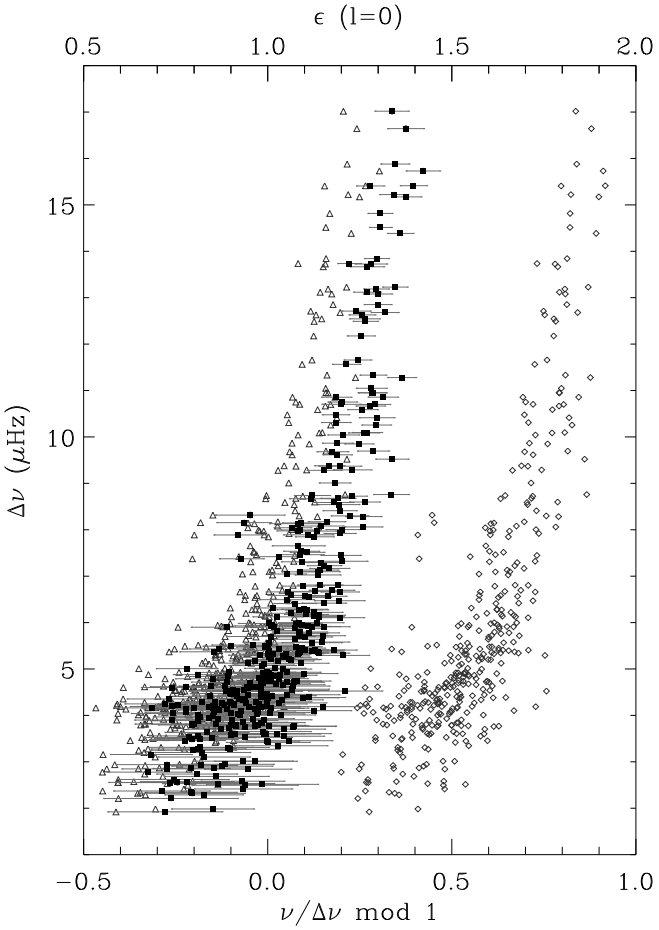

FIG. 8.— Mode ridge centroids as measured from the folded and collapsed power spectrum for $l = 0$ (black squares), $l = 1$ (grey diamonds) and $l = 2$ (grey triangles). Note that the upper abscissa label shows ϵ for $l = 0$ modes. Error bars are only shown for $l = 0$ for clarity.

in so-called C-D diagrams (Christensen-Dalsgaard 1988) in Figure 9. We also plot the frequency separation ratios $\delta\nu_{0l}/\Delta\nu$ which, according to models, are expected to be largely insensitive to surface layer effects (Roxburgh & Vorontsov 2003; Otí Floranes et al. 2005; Mazumdar 2005; Chaplin et al. 2005).

We can see in Figure 9a that $\delta\nu_{02}$ is an almost fixed fraction of $\Delta\nu$, which confirms the findings by Bedding et al. (2010b) for low-luminosity red giants. We obtain the following relation for the full range of $\nu_{\rm max}$:

$$\delta\nu_{02} = (0.121 \pm 0.001)\Delta\nu + (0.047 \pm 0.008)\,, \qquad (11)$$

in agreement with the relation found by Bedding et al. (2010b). We see a deviation from this linear relationship for stars with $\Delta\nu \lesssim 10\,\mu$Hz ($\nu_{\rm max} \lesssim 120\,\mu$Hz), which can be seen in Figure 9b as an increase of the ratio $\delta\nu_{02}/\Delta\nu$. Additionally, we observe an increased spread of $\delta\nu_{02}$, particularly for stars with $\Delta\nu \sim 4\,\mu$Hz. While most of this spread in the red clump is due to the much larger number of stars (see Figure 5) and the larger uncertainty in determining $\delta\nu_{02}$, we tested whether it could also be related to physical properties of the stars. C-D diagrams for red giants calculated from stellar models (T. R. White et al., in preparation) show that the expected range in $\delta\nu_{02}/\Delta\nu$

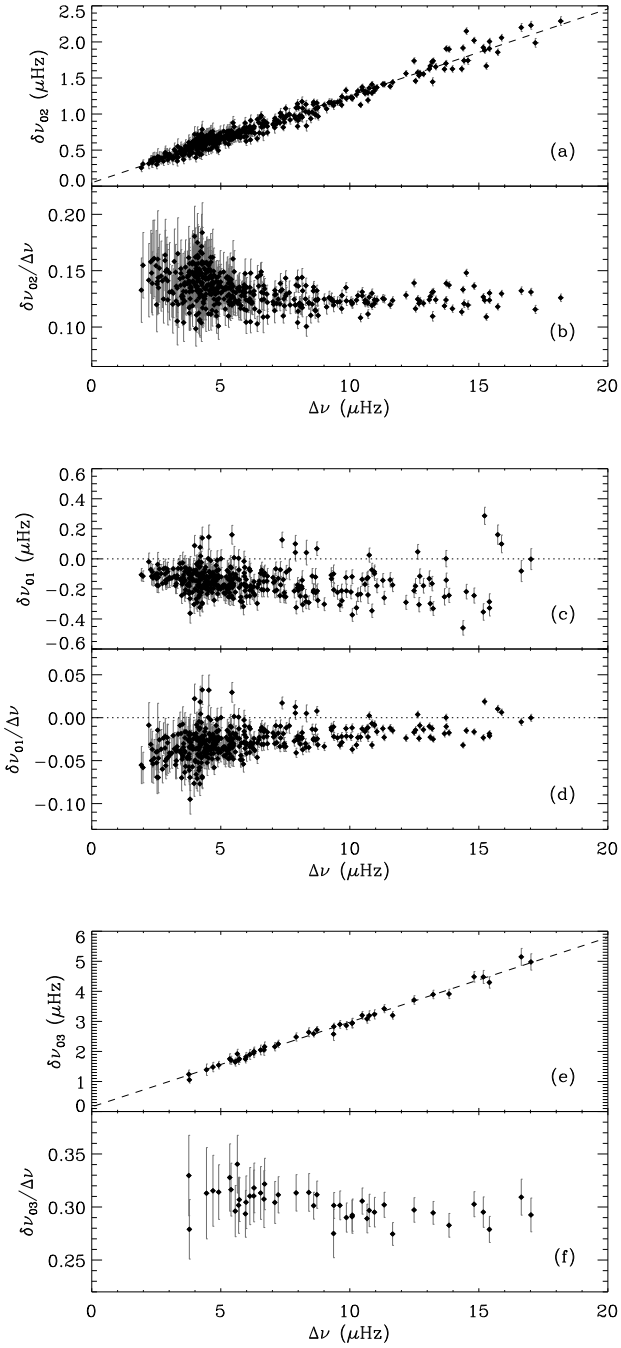

FIG. 9.— C-D diagram of $\delta\nu_{0l}$ versus $\Delta\nu$ for $l = 2$ (a), $l = 1$ (c) and $l = 3$ (e) and frequency separation ratios of $\delta\nu_{0l}/\Delta\nu$ for $l = 2$ (b), $l = 1$ (d) and $l = 3$ (f). Dashed lines in panels (a) and (e) show linear fits to the data.

for $M = 1 - 2\,M_\odot$ and solar metallicity in non He-core burning models is about 0.02, which is roughly comparable to the range of values observed in the data outside the red clump. Indeed, a comparison of stars with different $\delta\nu_{02}$ in the lower panel of Figure 6 has shown the spread can be partially explained by a spread in stellar masses, with lower-mass stars showing higher $\delta\nu_{02}$ values. More quantitative conclusions about the mass spread will be possible once the measurement uncertainties are reduced

by the collection of more data.

Figure 9c shows that $\delta\nu_{01}$ is negative for almost all red giants, confirming the findings by Bedding et al. (2010b). As for $l = 2$, we observe a trend (but with opposite sign) in the frequency separation ratio $\delta\nu_{01}/\Delta\nu$ with $\Delta\nu$, which can be seen in Figure 9d. The decrease of $\delta\nu_{01}/\Delta\nu$ and the increase of $\delta\nu_{02}/\Delta\nu$ appear to affect stars in the same range of $\Delta\nu$ and by a similar amount ($\sim$5%). Using stars common to both samples, we calculated a correlation coefficient of -0.1. While this indicates that the observed trends are statistically almost uncorrelated, we cannot at this point exclude that this is due to the large uncertainty of measuring $\delta\nu_{01}$.

As shown by Bedding et al. (2010b), the *Kepler* data allow the detection of $l = 3$ modes in red giants. We were able to measure the small separation $\delta\nu_{03}$ for 45 stars and a linear fit to the relation with $\Delta\nu$, shown in Figure 9e, yields:

$$\delta\nu_{03} = (0.282 \pm 0.005)\Delta\nu + (0.16 \pm 0.04)\,. \qquad (12)$$

Figure 9f shows the ratio $\delta\nu_{03}/\Delta\nu$, which shows some evidence for an increase of $\delta\nu_{03}$ with decreasing $\Delta\nu$. While the error bars appear to be too large to make any firm statements on this variation, the observed scatter suggests that the uncertainties are overestimated. Given that the relative amplitude of $l = 3$ modes is not well known, it seems likely that the strength of $l = 3$ modes has been considerably underestimated in the simulations used to derive the uncertainties.

4.3.3. *Ensemble collapsed échelle diagram*

In order to display the separations of the mode ridges for all stars, we use the measured values of ϵ to shift and align the folded and collapsed power spectra in an ensemble collapsed échelle diagram. The result is shown in the upper panel of Figure 10. Note that this diagram is slightly different from the scaled échelle diagram presented by Bedding et al. (2010b) in that we have *shifted* the folded and collapsed power spectra rather than *scaling* frequencies. The thick solid line in the lower panel shows the upper panel summed along the full range of $\nu_{\rm max}$. It clearly reveals the presence of ridges with $l = 0, 1, 2$, and also $l = 3$. The power for $l = 3$ is weaker than found by Bedding et al. (2010b), who considered a smaller sample of low-luminosity giants with high signal-to-noise. We attribute this to the larger (and less biased) sample of stars in this paper, including stars with undetectable $l = 3$ modes, as well as to the fact that the $l = 3$ ridge has a slight tilt, making its power spread out in the lower panel of Figure 10.

The trends of the frequency separation ratios observed in Figure 9 are clearly visible in Figure 10. As $\nu_{\rm max}$ (and hence $\Delta\nu$) decreases, the $l = 2$ ridge slopes to the left while the $l = 1$ ridge slopes to the right, corresponding to an increase of $\delta\nu_{02}/\Delta\nu$ and a decrease of $\delta\nu_{01}/\Delta\nu$. These features are also clearly shown by the thin red and blue lines in the lower panel of Figure 10, which correspond to subsets with $\nu_{\rm max} < 50\,\mu$Hz and $\nu_{\rm max} > 100\,\mu$Hz, respectively. The red and blue lines also show evidence for a slope of the $l = 3$ ridge, corresponding to an increase of $\delta\nu_{03}$ as observed in Figure 9f.

We note that the *relative* width of the $l = 0$ ridge shown in Figure 10 (measured in terms of $\Delta\nu$) decreases

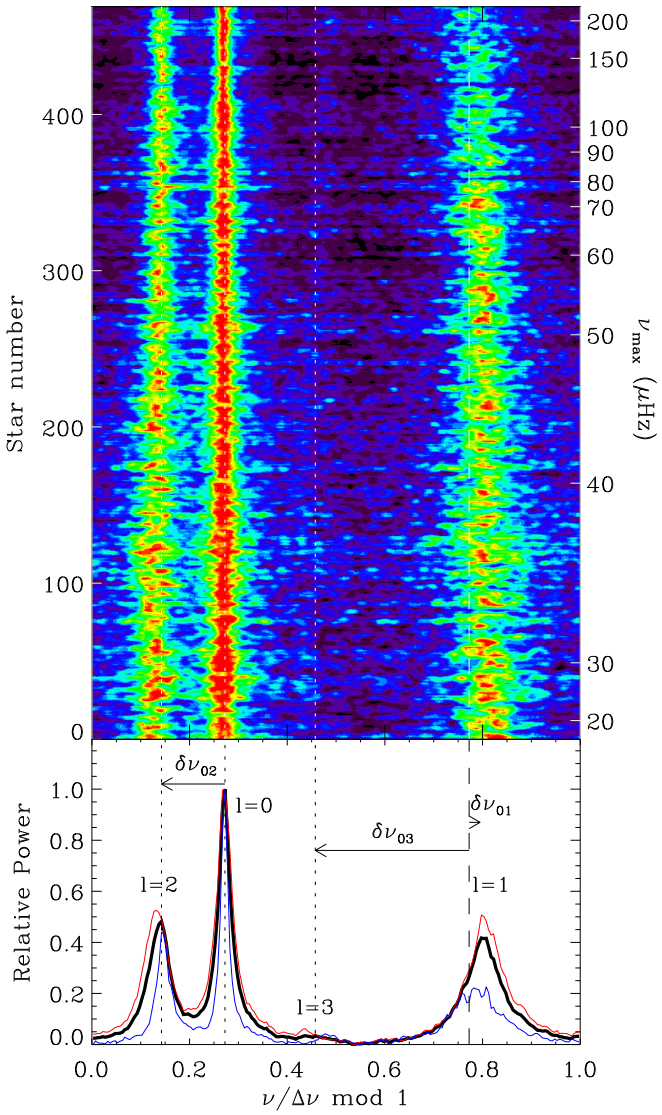

FIG. 10.— *Upper panel:* Ensemble collapsed échelle diagram of 470 red giants. Note that the contour threshold has been lowered to 40% of the maximum value and that each row shows the folded and collapsed power spectrum of one star. The right ordinate marks $\nu_{\rm max}$ values for selected rows. *Lower panel:* Upper panel collapsed along the entire range of $\nu_{\rm max}$ (thick black line) as well as in subsets $\nu_{\rm max} > 100\,\mu$Hz (thin blue line) and $\nu_{\rm max} < 50\,\mu$Hz (thin red line). Ridge identification and definitions of small separations used in this paper are indicated. In both panels, the dotted lines mark the centers of the $l = 0$, 2 and 3 ridge and the dashed line shows the midpoint of adjacent $l = 0$ modes.

with increasing $\nu_{\rm max}$. In fact, the *absolute* width of the ridge (in μHz), which is determined by the frequency resolution, mode lifetime and curvature, remains roughly constant over the range of stars considered. As found by Bedding et al. (2010b) for low-luminosity red giants, the $l = 1$ ridge is significantly broader than the others. This was interpreted as a direct confirmation of theoretical results by Dupret et al. (2009), which predicted complicated power spectra due to less efficient trapping of mixed modes in the cores of low-luminosity red giants. The models by Dupret et al. (2009) also predicted that this effect should become less pronounced for higher luminosity red giants. Indeed, we observe that the relative

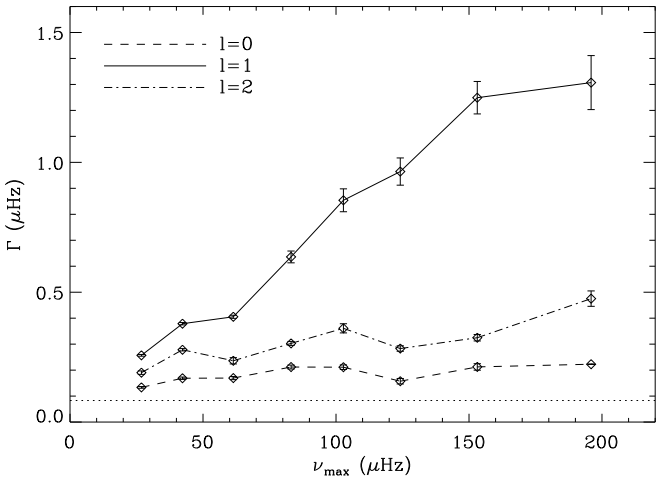

FIG. 11.— Absolute width of the $l = 0$ (dashed line), $l = 1$ (solid line) and $l = 2$ (dashed-dotted line) ridge as a function of $\nu_{\rm max}$. The dotted line marks the formal frequency resolution of the data (0.08 μHz).

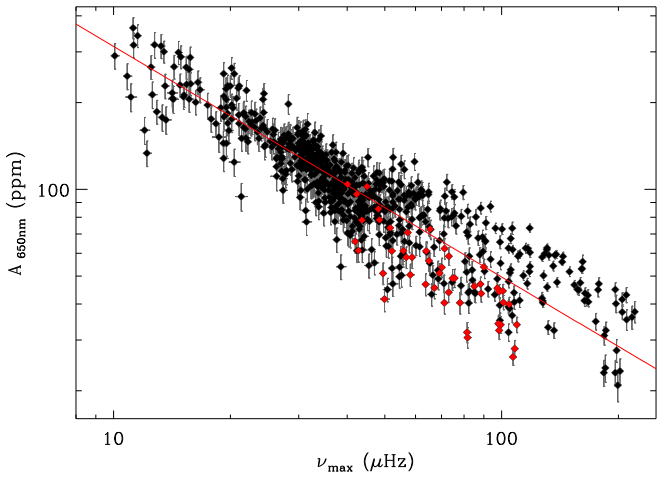

FIG. 12.— Pulsation amplitude versus $\nu_{\rm max}$ observed in the *Kepler* bandpass ($\lambda = 650$ nm). The red solid line shows a power law using a slope of -0.8. Red symbols show all stars with $\nu_{\rm max} > 40\,\mu$Hz and $M > 2M_{\odot}$ identified in Figures 6 and 7.

width of the $l = 1$ ridge shown in Figure 10 remains roughly constant, indicating that its absolute width is significantly lower for high-luminosity stars than for low-luminosity stars.

To quantify this, we measured the absolute widths of the $l = 0$, 1 and 2 ridges in several bins of $\nu_{\rm max}$, and show the result in Figure 11. Note that we have accounted for possible artificial broadening of the ridges due to Nyquist effects by excluding the two stars in our sample with $\nu_{\rm max} > 230\mu$Hz from this calculation. As can be seen in Figure 11, the widths of the $l = 0$ and 2 ridges remain roughly constant over the range of $\nu_{\rm max}$, while the width of the $l = 1$ ridge increases significantly. Our observation of a much narrower $l = 1$ ridge for high-luminosity stars therefore provides further confirmation of the results by Dupret et al. (2009).

4.4. *Pulsation amplitudes*

Amplitudes of solar-like oscillations provide valuable information to test models of convection (see Section 3.3). Equations (1), (7) and (8), in combination with effective temperatures, can be used to test theoretical scaling relations for amplitudes (see, e.g., Stello et al. 2007), as follows:

$$A_{\lambda} \propto T_{\rm eff}^{3.5s-r} \frac{\nu_{\rm max}^{-s}}{\lambda} \,. \qquad (13)$$

As shown by Mosser et al. (2010) for the *CoRoT* red giants, the relation between $\nu_{\rm max}$ and the pulsation amplitudes indeed follows a power law and this is shown for our *Kepler* sample in Figure 12. We have investigated the slope of the power law using amplitudes from four different methods (A2Z, COR, OCT and SYD, see Table 1 for references) and find on average:

$$A_{\rm 650nm} \propto \nu_{\rm max}^{-0.8} \,. \qquad (14)$$

As can be seen from Figure 12, the measured amplitudes show considerable structure, in particular a lack of low amplitudes for $\nu_{\rm max} \gtrsim 110\,\mu$Hz. This feature is found consistently in all methods and therefore appears to be intrinsic. Some low-amplitude stars do appear at $\nu_{\rm max} \gtrsim 180\,\mu$Hz, but we note that these amplitude estimates are rather uncertain due to the difficulty of estimating the background noise for stars oscillating near the Nyquist frequency. To investigate this lack of low amplitudes, we plot all stars that we have tentatively identified as secondary clump stars (using Figures 6 and 7, setting $\nu_{\rm max} > 40\,\mu$Hz and $M > 2M_{\odot}$) in Figure 12 as red symbols. We observe that these stars have systematically low amplitudes. We conclude that, for a given $\nu_{\rm max}$ in the range between $40 - 110\,\mu$Hz, stars with lower $\Delta\nu$ (and therefore higher mass, see Equation (10)) oscillate with lower amplitudes than other stars with the same $\nu_{\rm max}$. Assuming that this also holds for low-luminosity red giants, the lack of low amplitude stars for $\nu_{\rm max} \gtrsim 110\,\mu$Hz could then possibly be explained by the relatively fast evolution of more massive stars near the bottom of the red-giant branch compared to $\sim 1\,M_{\odot}$ stars.

Both the observation of low amplitudes for stars with lower $\Delta\nu$ in the range $\nu_{\rm max} \simeq 40 - 110\,\mu$Hz and the lack of low amplitude stars for $\nu_{\rm max} \gtrsim 110\,\mu$Hz indicate a significant dependence of the amplitude-$\nu_{\rm max}$ relation on the stellar mass. Since such a dependence is not seen in Equation (13), this suggests a revision of the scaling relation in Equation (7).

The overall distribution of the measured amplitudes in Figure 12 shows considerable additional scatter, which is possibly related to physical effects such as metallicity (Samadi et al. 2010a,b) in combination with measurement uncertainties. Tests have shown that the measurement error for amplitudes is dominated by the specific method and model used to subtract the background signal due to granulation and stellar activity. Further work is needed to identify possible systematic effects for the entire range of $\nu_{\rm max}$, which will then allow us to improve the relation between the oscillation amplitude and $\nu_{\rm max}$ using a large sample of stars on the giant branch.

5. SUMMARY AND CONCLUSIONS

Using data from the first four months of the *Kepler* mission we have studied various aspects of solar-like oscillations in $\sim$800 red giants. Our conclusions can be

summarized as follows:

1. The $\Delta\nu$-$\nu_{\rm max}$ relation using red giants is significantly different from the relation when main-sequence stars are included. This difference can be explained by evolutionary models and scaling relations, which show that the $\Delta\nu$-$\nu_{\rm max}$ relation is mainly sensitive to stellar masses for red giants and to metallicity for main-sequence stars.

2. The $\nu_{\rm max}$ and $\Delta\nu$ distributions are in qualitative agreement with a simple model of the stellar population. We observed that $\nu_{\rm max}$ for the red clump stars in the Kepler field is slightly higher than for the *CoRoT* fields, possibly due to the different stellar populations that are observed. We identified several stars with $\nu_{\rm max} = 40 - 110\,\mu$Hz and $M > 2M_{\odot}$, in agreement with a secondary clump population.

3. The quantity ϵ in the asymptotic relation is a function of $\Delta\nu$. If the relation between ϵ and fundamental parameters can be quantified and is also valid for main-sequence stars, it could be used to study surface layer effects or for mode identification in stars where ridges cannot be clearly identified due to short mode lifetimes or rotational splitting. We demonstrated the potential of the observed relation by providing mode identifications for four red giants observed by *CoRoT*.

4. We presented C-D diagrams for $l = 1$, 2 and 3 and show that frequency separation ratios of $\delta\nu_{02}/\Delta\nu$ and $\delta\nu_{01}/\Delta\nu$ reveal opposite trends as a function of $\Delta\nu$. We observed a spread in the small separations, in particular for stars in the red clump, and find evidence that this is partially due to the spread in mass. We also measured the small separation $\delta\nu_{03}$ and tentatively identify a similar variation of the frequency separation ratio $\delta\nu_{03}/\Delta\nu$ as observed for $\delta\nu_{02}/\Delta\nu$ as a function of $\Delta\nu$.

5. The absolute width of the $l = 1$ ridge for stars of higher luminosity is significantly narrower than for stars with low luminosity. This is the first quantitative confirmation of more efficient mode trapping as predicted by theory.

6. We presented a first estimate for the relation between pulsation amplitude and $\nu_{\rm max}$ for *Kepler* red giants. We observed a distinct lack of low-amplitude stars for $\nu_{\rm max} \gtrsim 110\,\mu$Hz and found that, for a given $\nu_{\rm max}$, stars with lower $\Delta\nu$ (and therefore higher mass, see Equation (10)) tend to show lower amplitudes than stars with higher $\Delta\nu$. Both observations can be explained with a mass dependence of the amplitude-$\nu_{\rm max}$ relation, and therefore suggest that the scaling relation for luminosity amplitudes of red giants needs to be revised.

The authors gratefully acknowledge the *Kepler* Science Team and all those who have contributed to the *Kepler* mission for their tireless efforts which have made these results possible. We are also thankful to A. Miglio for his kind help with the stellar population synthesis and to our anonymous referee for his/her helpful comments. Funding for the *Kepler* Mission is provided by NASA's Science Mission Directorate. DH acknowledges support by the Astronomical Society of Australia (ASA). DS and TRB acknowledge support by the Australian Research Council. The National Center for Atmospheric Research is a federally funded research and development center sponsored by the U.S. National Science Foundation. SH, YPE and WJC acknowledge support by the UK Science and Technology Facilities Council.

REFERENCES

Appourchaux, T., et al. 2008, A&A, 488, 705
Barban, C., et al. 2007, A&A, 468, 1033
Batalha, N. M., et al. 2010, ApJ, 713, L109
Bedding, T. R., & Kjeldsen, H. 2010, Communications in Asteroseismology, 161, 3
Bedding, T. R., et al. 2006, ApJ, 647, 558
—. 2010a, ApJ, 713, 935
—. 2010b, ApJ, 713, L176
Belmonte, J. A., Jones, A. R., Palle, P. L., & Roca Cortes, T. 1990, Ap&SS, 169, 77
Benomar, O., et al. 2009, A&A, 507, L13
Brown, T. M., & Gilliland, R. L. 1994, ARA&A, 32, 37
Brown, T. M., Gilliland, R. L., Noyes, R. W., & Ramsey, L. W. 1991, ApJ, 368, 599
Buzasi, D., Catanzarite, J., Laher, R., Conrow, T., Shupe, D., Gautier, III, T. N., Kreidl, T., & Everett, D. 2000, ApJ, 532, L133
Carrier, F., Eggenberger, P., & Bouchy, F. 2005, A&A, 434, 1085
Carrier, F., et al. 2010, A&A, 509, A73
Chaplin, W. J., Elsworth, Y., Miller, B. A., New, R., & Verner, G. A. 2005, ApJ, 635, L105
Christensen-Dalsgaard, J. 1988, in Proc. IAU Symp. 123, Advances in Helio- and Asteroseismology, ed. J. Christensen-Dalsgaard & S. Frandsen (Dordrecht: Kluwer), 295
Christensen-Dalsgaard, J. 2004, Sol. Phys., 220, 137
Christensen-Dalsgaard, J. 2008, Ap&SS, 316, 13
Christensen-Dalsgaard, J., & Frandsen, S. 1983, Sol. Phys., 82, 469
Christensen-Dalsgaard, J., & Perez Hernandez, F. 1992, MNRAS, 257, 62
Cochran, W. D. 1988, ApJ, 334, 349
De Ridder, J., Barban, C., Carrier, F., Mazumdar, A., Eggenberger, P., Aerts, C., Deruyter, S., & Vanautgaerden, J. 2006, A&A, 448, 689
De Ridder, J., et al. 2009, Nature, 459, 398
Deheuvels, S., et al. 2010, A&A, 515, A87
Dupret, M., et al. 2009, A&A, 506, 57
Edmonds, P. D., & Gilliland, R. L. 1996, ApJ, 464, L157
Frandsen, S., et al. 2002, A&A, 394, L5
García, R. A., et al. 2009, A&A, 506, 41
Gilliland, R. L. 2008, AJ, 136, 566
Gilliland, R. L., et al. 2010, PASP, 122, 131
Girardi, L. 1999, MNRAS, 308, 818
Girardi, L., Groenewegen, M. A. T., Hatziminaoglou, E., & da Costa, L. 2005, A&A, 436, 895
Gough, D. O. 1986, in Hydrodynamic and Magnetodynamic Problems in the Sun and Stars, ed. Y. Osaki, 117
Hekker, S., Barban, C., Baudin, F., De Ridder, J., Kallinger, T., Morel, T., Chaplin, W. J., & Elsworth, Y. 2010a, ArXiv e-prints
Hekker, S., et al. 2009, A&A, 506, 465
—. 2010b, A&A, submitted
—. 2010c, ApJ, 713, L187
—. 2010d, MNRAS, 402, 2049

Houdek, G., Balmforth, N. J., Christensen-Dalsgaard, J., & Gough, D. O. 1999, A&A, 351, 582
Huber, D., Stello, D., Bedding, T. R., Chaplin, W. J., Arentoft, T., Quirion, P., & Kjeldsen, H. 2009, Communications in Asteroseismology, 160, 74
Jenkins, J. M., et al. 2010, ApJ, 713, L120
Kallinger, T., Gruberbauer, M., Guenther, D. B., Fossati, L., & Weiss, W. W. 2010a, A&A, 510, A106
Kallinger, T., et al. 2008a, Communications in Asteroseismology, 153, 84
—. 2008b, A&A, 478, 497
—. 2010b, A&A, submitted
—. 2010c, A&A, 509, A77
Kjeldsen, H., & Bedding, T. R. 1995, A&A, 293, 87
Kjeldsen, H., et al. 2008, ApJ, 682, 1370
Latham, D. W., Brown, T. M., Monet, D. G., Everett, M., Esquerdo, G. A., & Hergenrother, C. W. 2005, in Bulletin of the American Astronomical Society, Vol. 37, Bulletin of the American Astronomical Society, 1340
Mathur, S., et al. 2010, A&A, 511, A46
Mazumdar, A. 2005, A&A, 441, 1079
Miglio, A., et al. 2009, A&A, 503, L21
Monet, D. G., Jenkins, J. M., Dunham, E. W., Bryson, S. T., Gilliland, R. L., Latham, D. W., Borucki, W. J., & Koch, D. G. 2010, ArXiv e-prints
Mosser, B., & Appourchaux, T. 2009, A&A, 508, 877
Mosser, B., et al. 2010, A&A, 517, A22
Otí Floranes, H., Christensen-Dalsgaard, J., & Thompson, M. J. 2005, MNRAS, 356, 671
Retter, A., Bedding, T. R., Buzasi, D. L., Kjeldsen, H., & Kiss, L. L. 2003, ApJ, 591, L151
Roxburgh, I. W., & Vorontsov, S. V. 2003, A&A, 411, 215
Samadi, R., Georgobiani, D., Trampedach R., R., Goupil, M. J., Stein, R. F., & Nordlund, A. 2007, A&A, 463, 297
Samadi, R., Ludwig, H., Belkacem, K., Goupil, M. J., & Dupret, M. 2010a, A&A, 509, A15
Samadi, R., et al. 2010b, A&A, 509, A16
Smith, M. A. 1983, ApJ, 265, 325
Stello, D., Bruntt, H., Preston, H., & Buzasi, D. 2008, ApJ, 674, L53
Stello, D., Chaplin, W. J., Basu, S., Elsworth, Y., & Bedding, T. R. 2009, MNRAS, 400, L80
Stello, D., & Gilliland, R. L. 2009, ApJ, 700, 949
Stello, D., et al. 2007, MNRAS, 377, 584
—. 2010, ApJ, 713, L182
Tarrant, N. J., Chaplin, W. J., Elsworth, Y., Spreckley, S. A., & Stevens, I. R. 2007, MNRAS, 382, L48
Tassoul, M. 1980, ApJS, 43, 469
Ulrich, R. K. 1986, ApJ, 306, L37
Yang, W., & Meng, X. 2010, New Astronomy, 15, 367
Yang, W., Meng, X., & Li, Z. 2010, ArXiv e-prints